

# Defining Solid Additive's Pivotal Role on Morphology Regulation in Organic Solar Cells Produced by Layer-by-layer Deposition

Weiwei Wu, Yongmin Luo, Top Archie Dela Peña, Jia Yao, Menoona Qammar, Mingjie Li, He Yan,\* Jiaying Wu,\* Ruijie Ma,\* and Gang Li

Herein, two emerging device optimization methods, solid additive and layer-by-layer (LBL) process, for organic solar cells (OSCs) are simultaneously studied. Through traditional blend cast and recently proposed identical solvent LBL cast, BDCB (2-monobromo-1,3-dichloro-benzene), a benzene derivative, is used to improve the device performance based on celebrity combination PM6:L8-BO. The results reveal that finely optimized BDCB concentration in PM6 solution can push the efficiency of LBL to 19.03% compared to blend cast with only 18.12% while the power conversion efficiency (PCE) changing trend is determined by BDCB's ratio in L8-BO's precursor. The morphology characterizations confirm there exists no significant stratification for LBL-processed devices, supported by a previously reported swelling-intercalation-phase separation (SIPS) model. Thereby, the solid additive's 2D optimization is considered a smart strategy for finely tuning the SIPS process, which results in various final morphology states. This work not only reports a cutting-edge efficiency for binary OSCs, but also new insight and deep understanding for LBL method-based morphology optimization strategy development.

innovation and device optimization efforts, enabling this eco-friendly, solution-processable, and aesthetically valuable photovoltaic (PV) technology more promising marketing prospect.<sup>[1–16]</sup> To further brighten the future of OSCs, efficiency enhancement based on photoactive layer morphology study and promotion is considered the key motivation, which includes many factors that matter such as basic property and fabrication methods of materials.<sup>[17–21]</sup> Apart from continuous material synthesis engineering, exploiting novel active layer deposition methods is also an important and effective way in recent years. Among all, volatile solid additive utilization and layer-by-layer (LBL) deposition have become the two most popular topics in pursuing ideal active layer morphology.<sup>[22–45]</sup> Solid additives are found powerful in realizing desired

## 1. Introduction

Single-junction organic solar cells (OSCs) started approaching 20% power conversion efficiency (PCE) due to material

crystallinity and phase separation, without enlarging the energy loss compared to liquid ones. Meanwhile, the LBL processing method is widely agreed to be effective in tuning the donor-acceptor vertical phase separation which is beneficial to


W. Wu, T. A. Dela Peña, J. Yao, H. Yan  
Department of Chemistry Department of Chemistry and Hong Kong  
Branch of Chinese National Engineering Research Center for Tissue  
Restoration and Reconstruction  
The Hong Kong University of Science and Technology  
Clear Water Bay, Hong Kong China  
E-mail: [hyan@ust.hk](mailto:hyan@ust.hk)

Y. Luo, T. A. Dela Peña, J. Wu  
Function Hub, Advanced Materials Thrust  
The Hong Kong University of Science and Technology  
Nansha, Guangzhou 511400, China  
E-mail: [jiayingwu@ust.hk](mailto:jiayingwu@ust.hk)

T. A. Dela Peña, M. Li  
Department of Applied Physics  
The Hong Kong Polytechnic University  
Hong Kong 999077, China

M. Qammar  
Department of Chemistry  
The Hong Kong University of Science and Technology (HKUST)  
Clear Water Bay Rd, Kowloon, Hong Kong 999077, China

R. Ma, G. Li  
Department of Electrical and Electronic Engineering  
Research Institute for Smart Energy (RISE)  
Photonic Research Institute (PRI)  
The Hong Kong Polytechnic University  
Hong Kong 999077, China  
E-mail: [ruijie.ma@polyu.edu.hk](mailto:ruijie.ma@polyu.edu.hk)

 The ORCID identification number(s) for the author(s) of this article can be found under <https://doi.org/10.1002/aenm.202400354>

© 2024 The Authors. Advanced Energy Materials published by Wiley-VCH GmbH. This is an open access article under the terms of the [Creative Commons Attribution](#) License, which permits use, distribution and reproduction in any medium, provided the original work is properly cited.

DOI: 10.1002/aenm.202400354

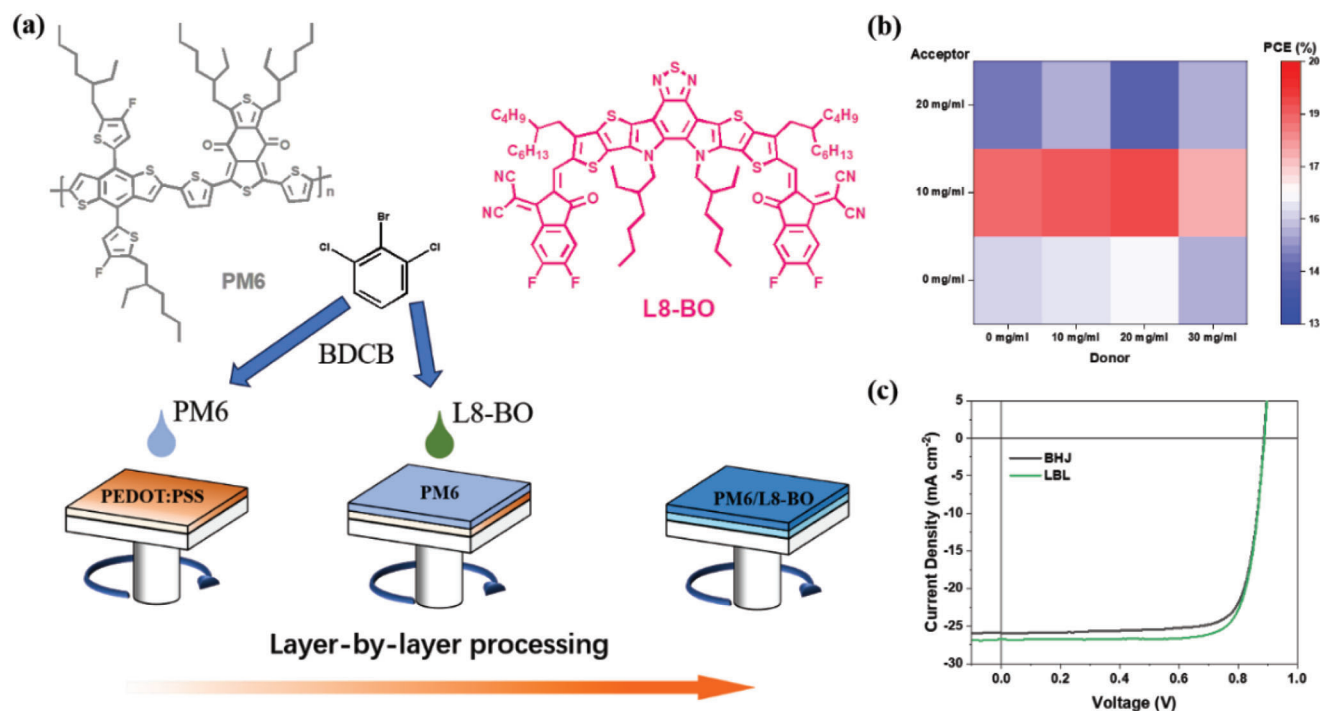


**Figure 1.** a) Chemical structure of photoactive materials and solid additive, and casting method scheme. b) Heat map summary for 2D optimization results of the LBL structured solar cells. c)  $J$ - $V$  characteristics of optimized BHJ and LBL devices.

suppressing bimolecular recombination thereby imparts better performance. Separately, these two methods already shine attractively; however, together are they believed to demonstrate synergistic effects for a more productive outcome.

Interestingly, solid additive strategy is usually applied in donor-acceptor blend bulk-heterojunction (BHJ), yet the only donor-additive or acceptor-additive interaction is considered as the morphology regulator.<sup>[46–48]</sup> Meanwhile, the more complicated donor-acceptor-additive has been rarely explored. On the LBL processing side, the use of additives on both donor and acceptor precursors simultaneously (either liquid or solid state) has been also inadequately discussed, not even taken as a scientific issue but more as an engineering technique.<sup>[49,50]</sup> Recently, some works focused on additive interaction with donor and acceptor for both BHJ and LBL films,<sup>[51,52]</sup> yet more systematic mechanism digging and in-depth understanding is still in shortage. Hence, implementing a comprehensive study on solid additive's morphological and photophysical tuning effect on the donor layer, acceptor layer, and obtained active layer in an LBL fabrication scenario, would be a scientifically inspiring effort and an efficiency-pushing candidate.

Herein, PM6/L8-BO which is a well-studied binary donor-acceptor system for LBL architecture,<sup>[53]</sup> and a halogenated solid additive BDCB (2-monobromo-1,3-dichloro-benzene) have been investigated. Specifically, a 2D optimization of additive's concentration in donor/acceptor solution has been carried out for LBL architecture in reference to BHJ/PM6:L8-BO. It is found that BDCB induces the formation of nanofiber network in PM6:L8-BO blend cast film, as well as tuned crystalline features and phase separation toward improved PCE. On the other hand, over-

dosing would cause over-aggregated L8-BO agglomerates without significant  $\pi$ - $\pi$  stacking signals (i.e., known to imparts poor charge transport and indecent device performance). For the LBL architectural active layers, BDCB's concentration in donor precursor is confirmed crucial to finely modulating the swelling-intercalation-phase separation (SIPS) process of L8-BO in the PM6 polymer matrix.<sup>[53]</sup> The concentration of BDCB in L8-BO solution is mainly correlated to its molecular packing, especially the  $\pi$ - $\pi$  stacking feature. Increasing BDCB concentration in PM6 can change the domain size and interval of its crystallites (i.e., quasi porous structure),<sup>[54]</sup> which would determine the final morphology of the active layer after the SIPS process. Consistent with previous reports, the LBL processed films exhibit no clear donor-acceptor vertical phase segregation. However, the in-plane phase separation size can be largely affected and likewise for the general crystallization behavior. Due to this more flexible morphology modulation, the optimized LBL device displays a better PCE than its BHJ counterpart does. This can be attributed to more suitable phase distribution and ordered molecular packing, facilitating improved charge generation and transport. As a result, a 19.03% efficiency is obtained, lying at the cutting-edge level for binary OSCs enabled by LBL fabrication.<sup>[23,55,56]</sup> This work not only proposes a novel solid additive for

**Table 1.** Photovoltaic performance of optimized BHJ and LBL devices.

PM6:L8-BO	$V_{OC}$ (V)	$J_{SC}$ (mA cm <sup>-2</sup> )	FF (%)	PCE (%)
Optimal BHJ	0.888	25.92	78.9	18.12
Optimal LBL	0.891	26.80	79.7	19.03

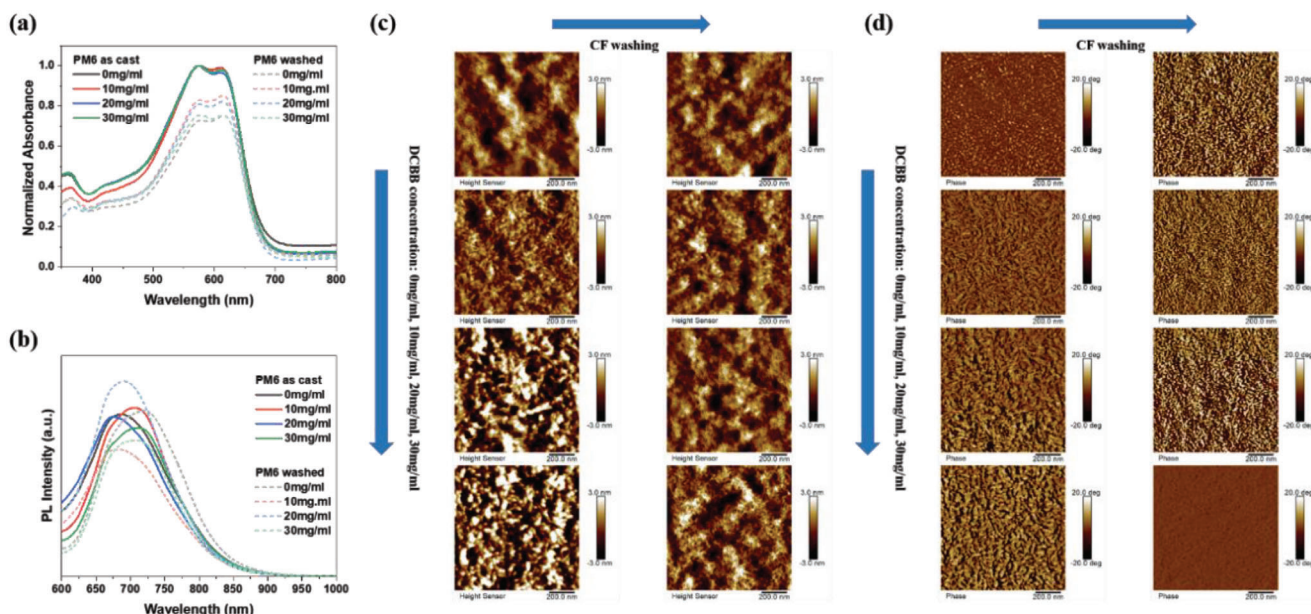


**Figure 2.** a) Normalized UV-vis absorption profiles and b) PL spectra of PM6 films, cast from precursors with different BDCB concentrations, with & without CF washing post treatment. The AFM c) height images and d) phase images of all these PM6 films.

effective morphology promotion and successfully applies solid additive into the 2D optimization for LBL type cells, but also reveals the underlying working mechanism of solid-additive participated SIPS process, and extends this model's understanding depth and importance.

## 2. Results and Discussion

A novel solid additive named 1,3-dichloro-2-monobromo-benzene (BDCB) is chosen as the research target of this work provided that its analogs are widely reported effective in tuning active layer morphology and improving PV performance.<sup>[24,29]</sup> The reference photoactive system is PM6:L8-BO, a well-known combination for both BHJ and LBL casted devices. Their chemical structures and device fabrication schematic diagram are illustrated in **Figure 1a**. The devices based on BHJ and LBL architectures of ITO/PEDOT:PSS/active layer /PNDIT-F3N/Ag are fabricated. The current density versus voltage ( $J$ - $V$ ) characteristics are presented in **Figure S1a** (Supporting Information) (BHJ), and **Figure S2** (Supporting Information) (LBL). The results are all demonstrated in **Table S1** (Supporting Information) and **Table 1**, as well as **Figure 1b** for visualizing the 2D LBL optimization details (comprehensive optimization of BDCB's content in both donor and acceptor precursors). To further compare the device performance of BHJ and LBL types of cells, the optimized  $J$ - $V$  curves are plotted in **Figure 1c**.

In a traditional BHJ scenario, the use of BDCB ( $10 \text{ mg mL}^{-1}$ ) can first increase the photovoltaic performance screened by the improved short-circuit current density ( $J_{SC}$ ) and fill factor ( $FF$ ), though slightly lower open-circuit voltage ( $V_{OC}$ ). Meanwhile, the overdosed BDCB ( $20 \text{ mg mL}^{-1}$ ) causes loss for all parameters leading to poorer PCE. The accuracy of device results is supported by external quantum efficiency (EQE) spectra in **Figure S1b** (Supporting Information), where the integrated current density values

are found 23.61, 25.12, and 23.25  $\text{mA cm}^{-2}$ , representing the error is within 5%. Turning to the LBL ones, no matter what concentrations are set for PM6 solutions, the performance changing rule follows that  $10 \text{ mg mL}^{-1} > 0 \text{ mg mL}^{-1} > 20 \text{ mg mL}^{-1}$  for BDCB's concentration in L8-BO. This implies that the dominant behavior is the crystallization of L8-BO. On the other hand, the ratio of BDCB in PM6 also significantly affects the efficiencies (from 18.57% to 18.61%, 19.03% and 17.44%). These measurements are also substantiated by the EQE spectra as plotted in **Figure S3** (Supporting Information). Overall, the LBL method with a more flexible solid additive treatment range taps the performance potential better than BHJ does, and its incorporation for both PM6 and L8-BO is vital for pursuing the best PCE. Empirically, the use of solid additives is supposed to tune the morphology toward different photovoltaic performances according to many studied BHJ cases, thus the understanding of LBL-enabled 2D optimization is also supposed to be gained by through morphological investigation.

Different from blend cast, the LBL processing includes a stage of solvent washing before the acceptor material is deposited onto the donor layer. Hence, the PM6 eigen-property is studied here through the simple-cast group and CF washed group, as demonstrated in **Figure 2**: normalized UV-vis absorption (2a), photoluminescence (2b) spectra, and atomic force spectroscopy height (2c) + phase (2d) images. Typically, PM6 is a pre-aggregated polymer in solution, thus the simple cast films demonstrate no significant differences. After CF washing, 10 and 20  $\text{mg mL}^{-1}$  BDCB treated films contain better absorbance, indicating proper solid additive incorporation leads to more crystalline PM6 in the film state. Besides, the transition of a higher 0-1 vibrational peak to a higher 0-0 peak supports that CF post-casting can move top side non-crystalline PM6. The CF washing is also found to result in different featured changes for the emission spectra of PM6, which indicates that BDCB-treated donor

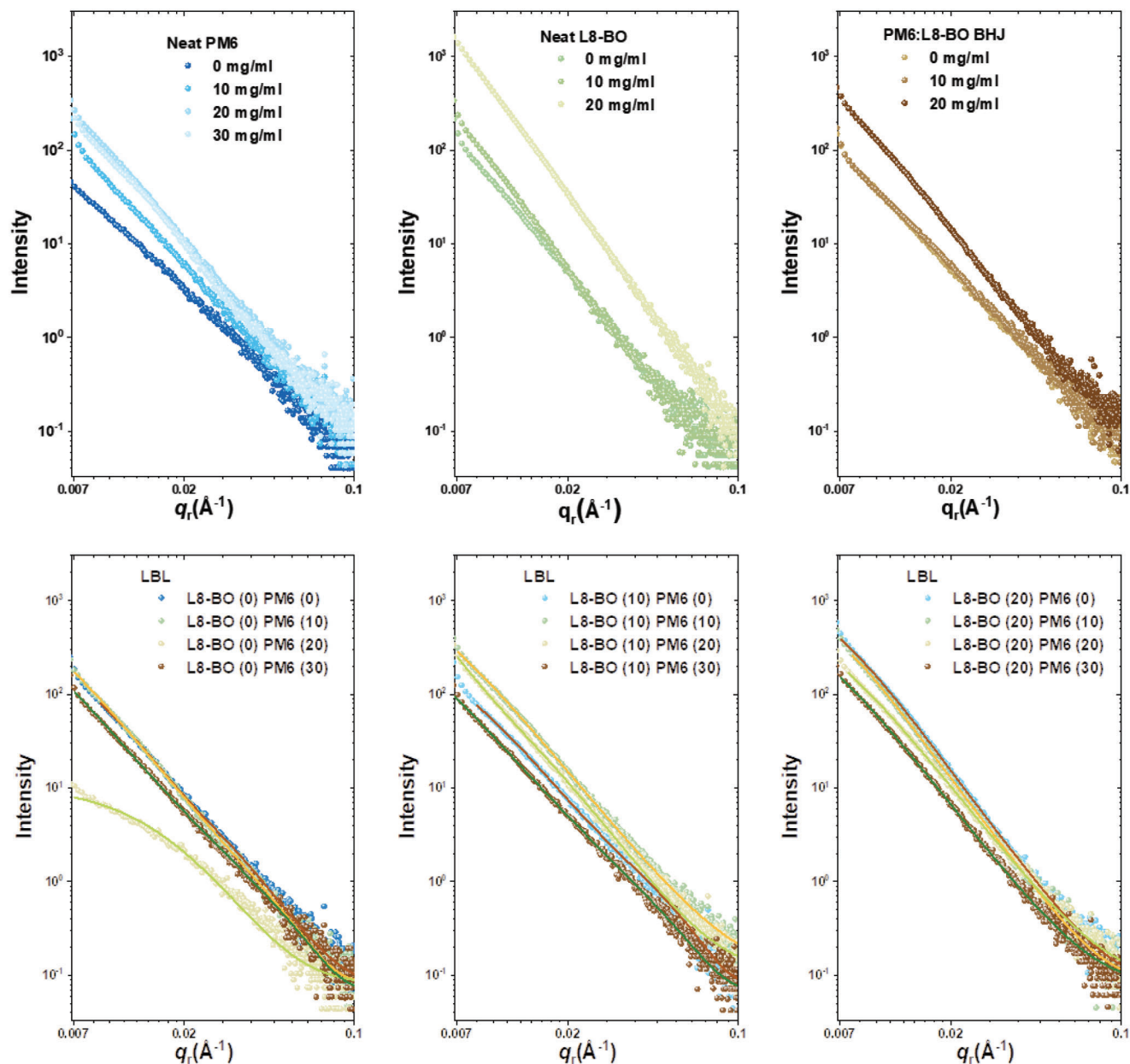


**Figure 3.** In-plane GISAXS intensity profiles and fitting lines of neat PM6 and L8-BO films, PM6:L8-BO blend cast films, LBL fabricated PM6:L8-BO films.

layers contain varied surface morphology and thus different crystalline/energetic variation after being washed by CF. According to the phase images, the use of BDCB can induce more nanofibrils for PM6, which becomes stronger and stronger with the increase of BDCB content. CF washing makes the surface of PM6 more sophisticated, but with 30 mg mL<sup>-1</sup> BDCB the nanofibrils in PM6 disappears. These results indicate that proper BDCB addition provides a porous structure in PM6 film, favorable for post-cast L8-BO molecules locating, crystallizing, swelling, and aggregating. Therefore, fine optimization of BDCB's concentration in the donor layer is a rational modulation of the SIPS process. Consistently, from Figure S4 (Supporting Information), it is unsurprisingly that 10 mg mL<sup>-1</sup> BDCB induces proper scale

molecule aggregates while 20 mg mL<sup>-1</sup> BDCB leads to oversized agglomerates. Thereafter, from Figures S5–S7 (Supporting Information), the AFM images indicate that 0 mg mL<sup>-1</sup> BDCB treated PM6 bottom layer results in the most significant interpenetrating nanofibril networks when horizontally compared the samples, regardless of BDCB ratio in L8-BO solution. Furthermore, the morphology tuning effect of BDCB in blend cast films is also screened by AFM experiments as shown in Figure S8 (Supporting Information): insignificant phase separation (0 mg mL<sup>-1</sup>), refined nanofibers (10 mg mL<sup>-1</sup>), and non-continuous aggregates (20 mg mL<sup>-1</sup>).

Subsequently, quantitative and more bulk-included analyses of phase separation are enabled by the grazing incidence

**Table 2.** Fitted GISAXS parameters for all films.

Films	$\varphi$ (%)	$\eta$ (nm)	D	2Rg (nm)	$\xi$ (nm)	L (nm)	2R (nm)
PM6 (0 mg mL <sup>-1</sup> )	16.0	16.5	2.65	72.6	/	/	/
PM6 (10 mg mL <sup>-1</sup> )	18.0	17.7	2.78	81.1	/	/	/
PM6 (20 mg mL <sup>-1</sup> )	16.5	18.1	2.85	84.8	/	/	/
PM6 (30 mg mL <sup>-1</sup> )	28.9	21.4	2.80	98.7	/	/	/
L8-BO (0 mg mL <sup>-1</sup> )	10.1	21.2	2.85	99.3	/	/	/
L8-BO (10 mg mL <sup>-1</sup> )	15.3	33.8	2.95	163.2	/	/	/
L8-BO 20 mg mL <sup>-1</sup> )	20.0	32.7	2.96	158.3	/	/	/
PM6:L8-BO (0 mg mL <sup>-1</sup> )	/	8.9	2.67	39.4	28.3	/	/
PM6:L8-BO (10 mg mL <sup>-1</sup> )	/	4.1	3.00	28.5	20.1	/	/
PM6:L8-BO 20 mg mL <sup>-1</sup> )	/	10.0	2.66	62.4	20.6	/	/
PM6 (0 mg mL <sup>-1</sup> )/L8-BO (0 mg mL <sup>-1</sup> )	/	/	/	/	18.9	510	6.6
PM6 (10 mg mL <sup>-1</sup> )/L8-BO (0 mg mL <sup>-1</sup> )	/	/	/	/	18.4	551	6.8
PM6 (20 mg mL <sup>-1</sup> )/L8-BO (0 mg mL <sup>-1</sup> )	/	/	/	/	46.5	394	7.8
PM6 (30 mg mL <sup>-1</sup> )/L8-BO (0 mg mL <sup>-1</sup> )	/	/	/	/	24.2	516	6.6
PM6 (0 mg mL <sup>-1</sup> )/L8-BO (10 mg mL <sup>-1</sup> )	/	/	/	/	23.9	476	6.3
PM6 (10 mg mL <sup>-1</sup> )/L8-BO (10 mg mL <sup>-1</sup> )	/	/	/	/	19.8	488	6.7
PM6 (20 mg mL <sup>-1</sup> )/L8-BO (10 mg mL <sup>-1</sup> )	/	/	/	/	21.2	440	6.1
PM6 (30 mg mL <sup>-1</sup> )/L8-BO (10 mg mL <sup>-1</sup> )	/	/	/	/	20.9	446	6.7
PM6 (0 mg mL <sup>-1</sup> )/L8-BO (20 mg mL <sup>-1</sup> )	/	15.0	2.92	71.7	38.2	/	/
PM6 (10 mg mL <sup>-1</sup> )/L8-BO (20 mg mL <sup>-1</sup> )	/	12.2	3.30	65.0	23.7	/	/
PM6 (20 mg mL <sup>-1</sup> )/L8-BO (20 mg mL <sup>-1</sup> )	/	14.3	3.00	70.0	36.4	/	/
PM6 (30 mg mL <sup>-1</sup> )/L8-BO (20 mg mL <sup>-1</sup> )	/	18.1	3.00	88.7	42.3	/	/

small-angle X-Ray (GISAXS) measurement.<sup>[57]</sup> The IP directional intensity profiles and corresponding fitting results are displayed in **Figure 3** and **Table 2**, respectively. Assisted by AFM phase images, and suggested by the fitting accuracy, the neat donor and acceptor films are analyzed through fractal model,<sup>[58]</sup> while the blend cast and L8-BO-20 mg mL<sup>-1</sup> LBL films are evaluated by Debye-Anderson-Brumberger (DAB) + fractal model,<sup>[59]</sup> lastly the LBL films of 0 and 10 mg mL<sup>-1</sup> BDCB in L8-BO solutions are studied by DAB & Flexible Cylinder model.<sup>[19]</sup> In different models, marks have their own interpretations.  $\eta$ , D,  $\xi$ , and  $\varphi$  refer to correlation length, aggregation's dimensionality, PM6-rich phase size, and crystalline phase ratio. L and 2R are special parameters for the cylinder model, representing the fiber length and diameter for the acceptor L8-BO. The 2Rg for neat films stands for crystalline aggregate scale and the size of L8-BO pure phase length scale in DAB+fractal model. Accordingly, PM6 film can be finely tuned by 10 and 20 mg mL<sup>-1</sup> BDCB treatment to achieve a desirable bottom layer for L8-BO's deposition, but 30 mg mL<sup>-1</sup> BDCB would result in dramatically increased crystalline phase and corresponding phase scale, leaving insufficient space for L8-BO molecules interpenetrate and aggregate, and thus incomplete SIPS. On the other hand, the crystalline ratio of L8-BO can be promoted from 10.1% to 20.0%, which is also consistent with AFM phase images. Intrinsically formed high-ratio crystallite is supposed to be the reason for aggregates replacing nanofibers in L8-BO-20 mg mL<sup>-1</sup> LBL films compared to those based on L8-BO-0 and -10 mg mL<sup>-1</sup>. Observably, in LBL films with fibrillated structure, the lengths are several times longer than 100 nm (film thickness) while the diameters of L8-BO fiber are similar which supports efficient D/A interface charge separation and

charge transport in pure domains. On the contrary, LBL films with 20 mg mL<sup>-1</sup> BDCB in L8-BO exhibit very large L8-BO phase scales (71.7, 65.0, 70.0, and 88.7 nm), as well as multiplied PM6-rich domain sizes. Such over-separated phase distribution well explains sacrificed  $J_{SC}$  and  $FF$ . Meanwhile, for blend cast (BHJ) films, the effect of using BDCB in phase separation modulation is revealed where the optimal film has the most balanced and finest PM6-rich and L8-BO crystalline phase scales, that are beneficial to improve D/A interface area.

Aside from general phase separation, the molecular packing, crystallization behavior, and donor-acceptor vertical segregation are subsequently studied through grazing incidence wide angle X-Ray scattering (GIWAXS) experiment.<sup>[60–62]</sup> Herein, 0.2° X-ray incidence is used for neat PM6 and L8-BO films, as well as BHJ and LBL films, while 0.05° X-ray incidence is applied for LBL films to investigate the vertical phase segregation.<sup>[63]</sup> The 2D GIWAXS patterns and corresponding line cuts alongside in-plane (IP) and out-of-plane (OOP) orientations are displayed from **Figures S9–S15** (Supporting Information). Focusing on OOP directional  $\pi$ - $\pi$  stacking, the calculated crystalline parameters, d-spacing and coherence length (CL), are demonstrated in **Figure 4**. According to these figures, the crystalline characteristics of PM6 and L8-BO can be initially judged wherein PM6 exhibits d-spacings between 3.75 and 3.8 Å, while L8-BO displays d-spacings less than 3.7 Å. The BDCB ratio in solution cannot change the d-spacing and CL values of PM6 a lot. However, the 10 mg mL<sup>-1</sup> BDCB significantly increases the CL with reduced d-spacing for L8-BO. Moreover, 20 mg mL<sup>-1</sup> BDCB leads to the disappearance of  $\pi$ - $\pi$  stacking peak for L8-BO, and lamellar peaks show clear shifts. These results can explain the poor device

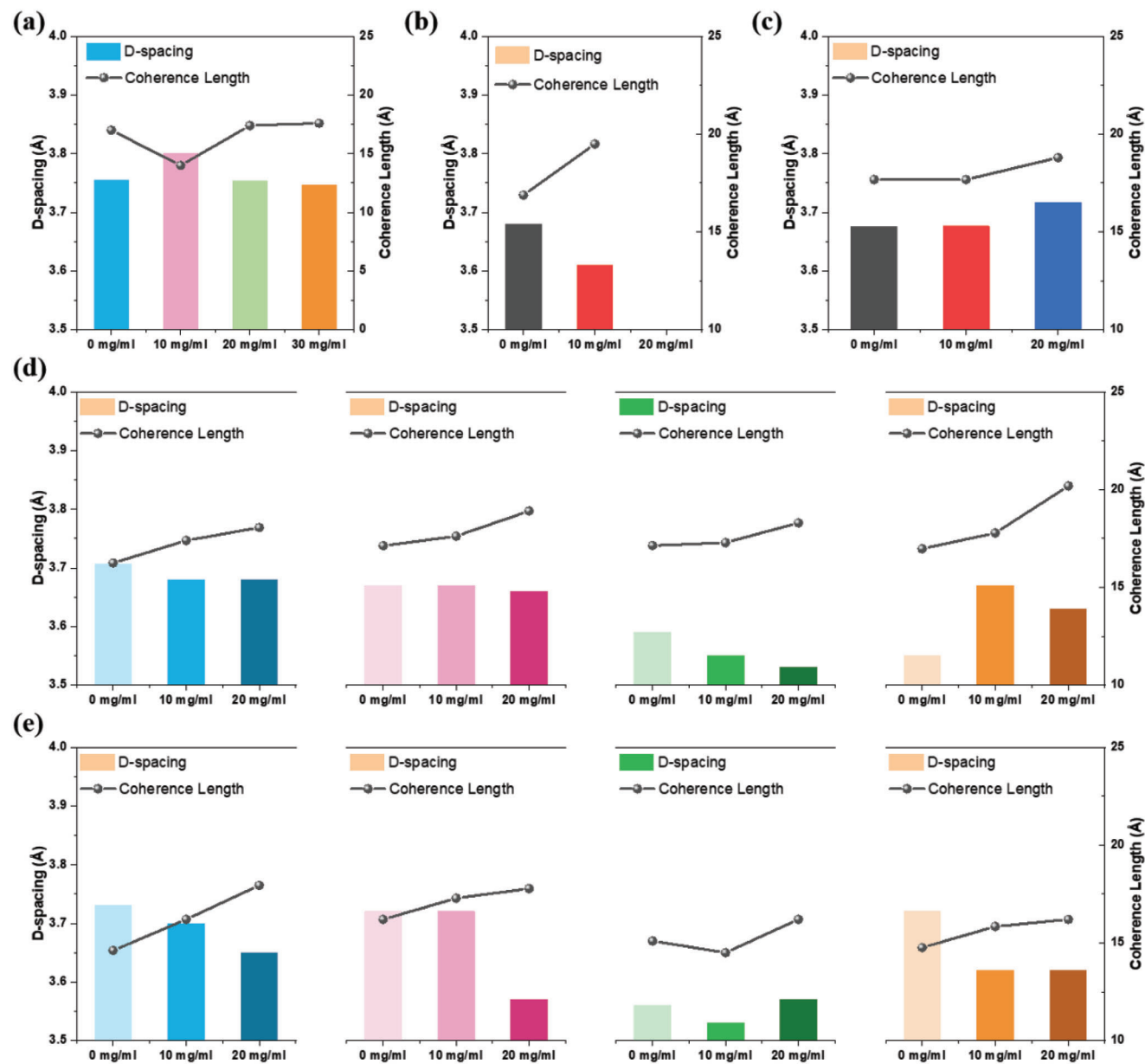


**Figure 4.** Fitted GIWAXS parameters for OOP directional  $\pi$ - $\pi$  stacking peaks following varied BDCB concentrations: a) PM6 neat films, b) L8-BO neat films, c) PM6:L8-BO blend cast films, and LBL processed PM6/L8-BO films of d) 0.2° X-ray detection [bulk] and e) 0.05° X-ray detection [top part].

performance when BDCB concentration comes to 20 mg mL<sup>-1</sup>, together with previously revealed oversized L8-BO clusters. The fitted parameters for blend cast PM6:L8-BO films reveal their  $\pi$ - $\pi$  stacking is mainly contributed by small molecule acceptor L8-BO, since their d-spacings are at the range of 3.65–3.7 Å. Notably, for 20 mg mL<sup>-1</sup> BDCB processed blend cast film, the d-spacing value surpasses 3.7 Å, which is supposed to be attributed to BDCB overdosing undermining L8-BO's  $\pi$ - $\pi$  stacking, thus herein blend film's (010) peak signal is mainly generated from PM6 crystallites. The bulk GIWAXS results of LBL films demonstrate that changing the BDCB content in L8-BO solution can less effectively tune the d-spacing than regulating the concentration in the PM6 precursor. This means the aggregated and crystalline prop-

erty of PM6 is of high importance for the final blend film morphology. This is consistent with the SIPS process prediction of insignificant donor-acceptor stratification but well-gained global interpenetration.<sup>[51]</sup> When the PM6 layer processing comes to 20 mg mL<sup>-1</sup> BDCB content, the d-spacings are reduced to smaller than 3.6 Å. The tightened stacking is considered beneficial to charge transport, and facilitating exciton diffusion for more efficient charge generation. Compared to bulk LBL's GIWAXS patterns (Figure S12, Supporting Information), the 0.05° incidence obtained patterns in Figure S13 (Supporting Information) displays less features of L8-BO: vice lamellar peaks at  $\approx 0.4$  Å<sup>-1</sup> disappear. Therefore, though L8-BO is cast after the deposition of PM6, the final LBL blend films contain more PM6 at the top. The

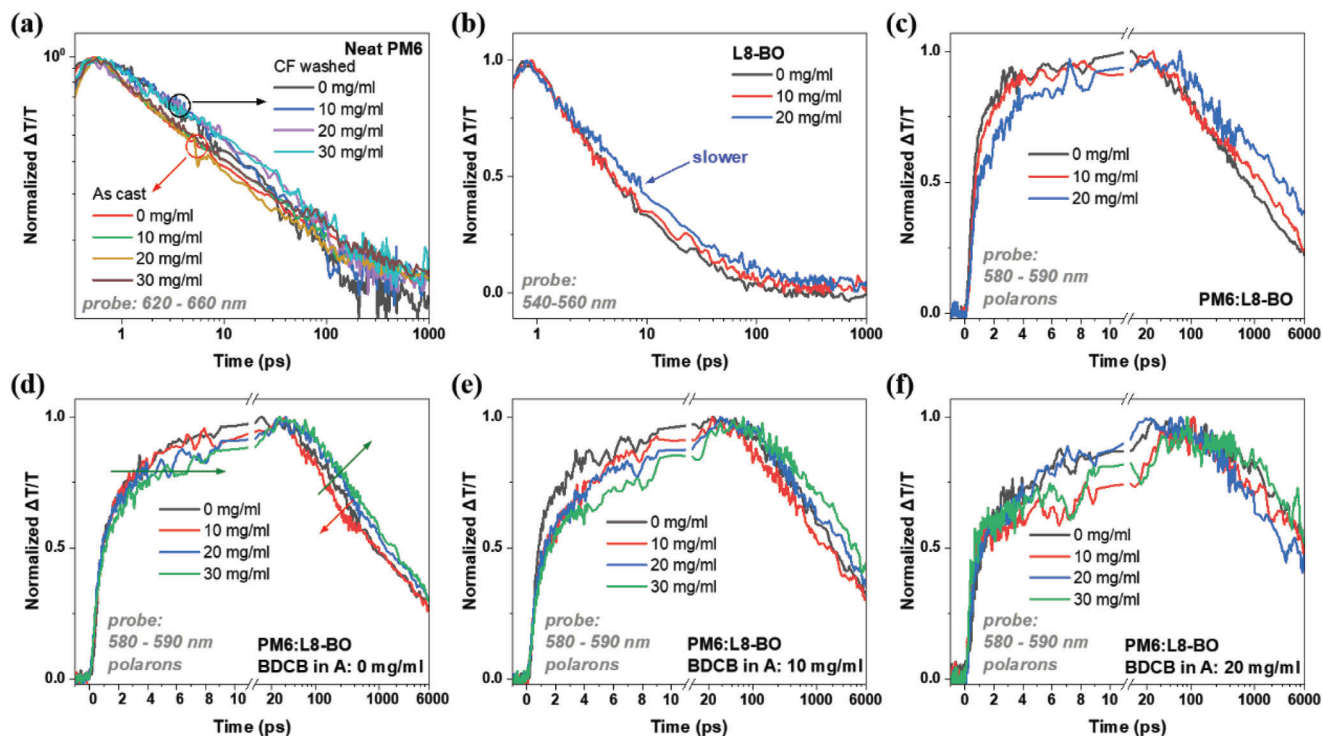


**Figure 5.** Singlet excitons decay in a) neat PM6 films before and after CF washing, and b) neat L8-BO films. Polaron dynamics in c) blend cast films, d) L8-BO-0 mg mL<sup>-1</sup> based LBL films, e) L8-BO-10 mg mL<sup>-1</sup> based LBL films, and f) L8-BO-20 mg mL<sup>-1</sup> based LBL films. Samples are pumped with either 800 nm (neat acceptor and blend films) or 400 nm (neat donor films) fs-laser under a fluence of 3  $\mu\text{J cm}^{-2}$  and the change in absorption is probed using a white light continuum.

guess of SIPS mechanism and the reliability of IP GISAXS intensity enabled phase separation analysis are well substantiated.

Following the crystalline characteristic investigation, the corresponding charge transport ability of the photovoltaic blend is evaluated by the space charge limited current (SCLC) method,<sup>[64–66]</sup> for which a bunch of hole-only and electron-only devices are fabricated. The  $J$ - $V$  curves and extracted mobility values are exhibited in Figures S16, S17, and Table S2 (Supporting Information). The mobility variation trend is generally consistent with  $\pi$ - $\pi$  stacking parameter's changing characteristics: proper BDCB can induce better crystallization thus improving hole and electron mobility ( $\mu_h$ ,  $\mu_e$ ). Too high BDCB content reduces PM6's aggregation (possibly due to poorer crystallinity) and sacrifices L8-BO's  $\pi$ - $\pi$  stacking, so decreased mobility results are obtained. Optimized LBL (PM6-20 mg mL<sup>-1</sup>, L8-BO-10 mg mL<sup>-1</sup>) has a higher and more balanced ( $\mu_h$ ,  $\mu_e$ ) combination than optimized BHJ film does, which is supportive to the device performances of them.

With well-discussed morphology concerns, the device performance is subsequently correlated to corresponding photophysical properties as well, with the help of transient absorption spectroscopy (TAS) experiment.<sup>[67–69]</sup> The obtained TAS results are presented in both pseudo-2D contour maps and from representative spectral line cuts at various pump-probe delay times Figures S18–S22 (Supporting Information). The corresponding singlet excitons and polarons dynamics studies are extracted and shown in Figure 5. The singlet exciton decay dynamics for PM6 processed by different BDCB ratios are overall identical, while CF

washing can uniformly lead to a longer donor exciton lifetime based on Figure 5a. A prolonged lifetime is beneficial to charge separation by suppressing the geminate recombination. Meanwhile, from Figure 5b, 10 mg mL<sup>-1</sup> BDCB can slightly improve the exciton lifetime, as well, which is possibly due to improved crystalline order of  $\pi$ - $\pi$  stacking. On the contrary, though  $\pi$ - $\pi$  stacking is nearly undermined by 20 mg mL<sup>-1</sup> BDCB, its neat film's exciton lifetime is significantly longer than those of the other two. This can be taken as the result of a much higher crystalline phase ratio. Then attention is paid to active layers processed from blend casting (BHJ) (Figure 5c) and LBL methods (Figure 5d–f; Figure S23, Supporting Information). In the BHJ scenario, increasing additive content is positive in pursuing slower polaron sub-ns recombination dynamics, which is beneficial to 10 mg mL<sup>-1</sup> BDCB treated devices though 20 mg mL<sup>-1</sup> BDCB-based solar cell performance is poorer, because the latter one doesn't share similar morphology architecture as 0 and 10 mg mL<sup>-1</sup> BDCB treated blend film do thereby indicative of increasing in charge losses beyond sub-ns regime typically due to traps. Further, the slower exciton generation process by solid additive content's increase also follows the same pattern. As for LBL devices, as suggested by Figure S23 (Supporting Information), increasing the acceptor additive concentration leads to slower polarons generation dynamics and slower sub-ns polarons recombination, similar with BHJ's trend, therefore the understanding and underlying mechanism shall be similar, too. Meanwhile, from the side of the donor PM6's BDCB concentration variation, some differences take place. 10 mg mL<sup>-1</sup> donor additive

concentration always leads to faster sub-ns recombination making  $20 \text{ mg mL}^{-1}$  the most ideal case wherein the polarons recombination is not harmed for most of the cases while without oversaturating the BDCB concentration Overall, TAS results indicate that the increasing excitonic lifetimes in combination with unharmed sub-ns polarons recombination dynamics at appropriate additive concentrations for the donor and acceptor can lead to enhanced photocurrent generation, as observed from  $J_{\text{SC}}$ . On the other hand, suppression of free charge recombination beyond the sub-ns regime which highly influences the FF can be understood from nanomorphology and device physics which indicate better transport properties through the proper content of BDCB.

At last, as a supplement for TAS characterizations, some device physics experiments are carried out: photo-current versus effective voltage ( $J_{\text{ph}}$  vs  $V_{\text{eff}}$ ), light intensity dependent  $J_{\text{SC}}$  and  $V_{\text{OC}}$ . The results are displayed in Figures S24–S27 (Supporting Information) for BHJ and LBL devices. The calculated parameters including saturated current density ( $J_{\text{sat}}$ ), charge dissociation efficiency ( $\eta_{\text{diss}}$ ), charge collection efficiency ( $\eta_{\text{coll}}$ ), bimolecular recombination index ( $S$ ), and ideal diode factor ( $n$ ) are summarized in Table S3 (Supporting Information). The analysis methods for them are given in Supporting Information with details. The charge dissociation rates are uniformly similar for all kinds of PM6:L8-BO devices, thereby the  $J_{\text{SC}}$  improvement is mainly contributed by promoted  $J_{\text{sat}}$ , in other words, increased D/A interface area. On the other hand, very similar recombination parameters cannot present more information than a polaron dynamics study can.

### 3. Conclusion

In summary, driven by the curiosity of exploring emerging solid additives with halogen-phenyl type for morphological tuning effect on both donor and acceptor, a 2D optimization of additive concentration (i.e., BDCB herein) in PM6 and L8-BO precursors for LBL devices is carried out. The solar cell performance indicates that BDCB content in L8-BO plays a critical role in realizing high PCE, while its ratio in PM6 can tune the morphology and device efficiency in a more sophisticated way which further advances the PCE from 18.12% (blend cast) to 19.03%. The synergistic modulation (donor and acceptor precursors) is found in a refined tuning engineering of the previously confirmed SIPS process. This work presents a systematic studying case upon morphology evolution of OSCs, and demonstrates a new possibility of pursuing PCEs, thus boosting the future of achieving carbon neutrality.<sup>[70,71]</sup>

### Supporting Information

Supporting Information is available from the Wiley Online Library or from the author.

### Acknowledgements

R.M. thanks the support from PolyU Distinguished Postdoc Fellowship (1-YW4C). H.Y. appreciates the support from the National Key

Research and Development Program of China (No. 2019YFA0705900) funded by MOST, the Basic and Applied Research Major Program of Guangdong Province (No. 2019B030302007), the Shen Zhen Technology and Innovation Commission through (Shenzhen Fundamental Research Program, JCYJ20200109140801751), the Hong Kong Research Grants Council (research fellow scheme RFS2021-6S05, RIF project R6021-18, CRF project C6023-19G, GRF project 16310019, 16310020, 16309221, and 16309822), Hong Kong Innovation and Technology Commission (ITC-CNERC14SC01), Foshan-HKUST (Project NO. FSUST19-CAT0202), Zhongshan Municipal Bureau of Science and Technology (NO.ZSST20SC02) and Tencent Explorer Prize. J.W. thanks the Guangdong government and the Guangzhou government for funding (2021QN02C110), the Guangzhou Municipal Science and Technology Project (No. 2023A03J0097 and No. 2023A03J0003), and NSFC (52303249). G.L. thanks the support from Research Grants Council of Hong Kong (Project Nos 15221320, 15307922, C5037-18G, C4005-22Y), RGC Senior Research Fellowship Scheme (SRFS2223-5S01), the Hong Kong Polytechnic University: Sir Sze-yuen Chung Endowed Professorship Fund (8-8480), RISE (Q-CDBK), PRI (Q-CD7X), G-SAC5 and Guangdong-Hong Kong-Macao Joint Laboratory for Photonic-Thermal-Electrical Energy Materials and Devices (GDSTC No. 2019B121205001). H.Y. also acknowledges the support from HKUST Materials Characterization and Preparation Facility (MCPF). J. Wu also thanks the support from HKUST Materials Characterization and Preparation Facility Guangzhou (MCPF-GZ).

### Conflict of Interest

The authors declare no conflict of interest.

### Author Contributions

W.W., Y.L., and T.A.D.P. contributes equally to this work. W.W. performed investigation, formal analysis, methodology, conceptualization. Y.L. performed investigation, formal analysis. T.A.D.P. performed investigation, formal analysis, writing-original draft. J.Y. performed investigation and methodology. Y.W. performed investigation, writing-original draft. M.L., H.Y., J.W., and G.L. validated the resources. H.Y. and J.W. acquired funding acquisition and supervision. R.M. performed conceptualization, project administration, methodology, writing-original draft, writing-review & editing, supervision.

### Data Availability Statement

The data that support the findings of this study are available from the corresponding author upon reasonable request.

### Keywords

layer-by-layer, morphology, organic solar cells, solid additive

Received: January 22, 2024  
Revised: February 19, 2024  
Published online: March 8, 2024

- [1] T. Chen, S. Li, Y. Li, Z. Chen, H. Wu, Y. Lin, Y. Gao, M. Wang, G. Ding, J. Min, Z. Ma, H. Zhu, L. Zuo, H. Chen, *Adv. Mater.* **2023**, *35*, 2300400.
- [2] X. Xu, W. Jing, H. Meng, Y. Guo, L. Yu, R. Li, Q. Peng, *Adv. Mater.* **2023**, *35*, 2208997.
- [3] B. Zou, W. Wu, T. A. Dela Peña, R. Ma, Y. Luo, Y. Hai, X. Xie, M. Li, Z. Luo, J. Wu, C. Yang, G. Li, H. Yan, *Nano-Micro Lett.* **2023**, *16*, 30.



- [4] X. Kong, L. Zhan, S. Li, S. Yin, H. Qiu, Y. Fu, X. Lu, Z. Chen, H. Zhu, W. Fu, H. Chen, *Chem. Eng. J.* **2023**, 473, 145201.
- [5] H. Zhu, Y. Li, *Green Carbon*. **2023**, 1, 14.
- [6] Z. Chen, J. Zhu, D. Yang, W. Song, J. Shi, J. Ge, Y. Guo, X. Tong, F. Chen, Z. Ge, *Energy Environ. Sci.* **2023**, 16, 3119.
- [7] W. Wei, C. e. Zhang, Z. Chen, W. Chen, G. Ran, G. Pan, W. Zhang, P. Müller-Buschbaum, Z. Bo, C. Yang, Z. Luo, *Angew. Chem., Int. Ed.* **2024**, 63, 202315625.
- [8] X. Ma, G. Ran, H. Li, Y. Liu, X. Cui, H. Lu, Z. Yin, D. Li, H. Zhang, W. Liu, J. Yu, Y. Lin, Y. Liu, W. Zhang, G. Lu, L. Bo, P. Cheng, Z. Ma, Z. Bo, *Adv. Energy Mater.* **2023**, 13, 2302554.
- [9] C. Wang, X. Ma, Y.-f. Shen, D. Deng, H. Zhang, T. Wang, J. Zhang, J. Li, R. Wang, L. Zhang, Q. Cheng, Z. Zhang, H. Zhou, C. Tian, Z. Wei, *Joule*. **2023**, 7, 2386.
- [10] K. Liu, Y. Jiang, F. Liu, G. Ran, F. Huang, W. Wang, W. Zhang, C. Zhang, J. Hou, X. Zhu, *Adv. Mater.* **2023**, 35, 2300363.
- [11] C. Han, J. Wang, S. Zhang, L. Chen, F. Bi, J. Wang, C. Yang, P. Wang, Y. Li, X. Bao, *Adv. Mater.* **2023**, 35, 2208986.
- [12] Z. Zhong, S. Chen, J. Zhao, J. Xie, K. Zhang, T. Jia, C. Zhu, J. Jing, Y. Liang, L. Hong, S. Zhu, D. Ma, F. Huang, *Adv. Energy Mater.* **2023**, 13, 2302273.
- [13] X. Li, X. Kong, G. Sun, Y. Li, *eScience*. **2023**, 3, 100171.
- [14] Y. Liu, B. Liu, C.-Q. Ma, F. Huang, G. Feng, H. Chen, J. Hou, L. Yan, Q. Wei, Q. Luo, Q. Bao, W. Ma, W. Liu, W. Li, X. Wan, X. Hu, Y. Han, Y. Li, Y. Zhou, Y. Zou, Y. Chen, Y. Li, Y. Chen, Z. Tang, Z. Hu, Z.-G. Zhang, Z. Bo, *Sci. China Chem.* **2022**, 65, 224.
- [15] Y. Liu, B. Liu, C.-Q. Ma, F. Huang, G. Feng, H. Chen, J. Hou, L. Yan, Q. Wei, Q. Luo, Q. Bao, W. Ma, W. Liu, W. Li, X. Wan, X. Hu, Y. Han, Y. Li, Y. Zhou, Y. Zou, Y. Chen, Y. Li, L. Meng, Y. Li, Y. Chen, Z. Tang, Z. Hu, Z.-G. Zhang, Z. Bo, *Sci. China Chem.* **2022**, 65, 1457.
- [16] R. Ma, X. Jiang, J. Fu, T. Zhu, C. Yan, K. Wu, P. Müller-Buschbaum, G. Li, *Energy Environ. Sci.* **2023**, 16, 2316.
- [17] C. Li, X. Gu, Z. Chen, X. Han, N. Yu, Y. Wei, J. Gao, H. Chen, M. Zhang, A. Wang, J. Zhang, Z. Wei, Q. Peng, Z. Tang, X. Hao, X. Zhang, H. Huang, *J. Am. Chem. Soc.* **2022**, 144, 14731.
- [18] K. Gao, W. Deng, L. Xiao, Q. Hu, Y. Kan, X. Chen, C. Wang, F. Huang, J. Peng, H. Wu, X. Peng, Y. Cao, T. P. Russell, F. Liu, *Nano Energy*. **2016**, 30, 639.
- [19] D. Li, N. Deng, Y. Fu, C. Guo, B. Zhou, L. Wang, J. Zhou, D. Liu, W. Li, K. Wang, Y. Sun, T. Wang, *Adv. Mater.* **2023**, 35, 2208211.
- [20] Z. Wang, K. Gao, Y. Kan, M. Zhang, C. Qiu, L. Zhu, Z. Zhao, X. Peng, W. Feng, Z. Qian, X. Gu, A. K. Y. Jen, B. Z. Tang, Y. Cao, Y. Zhang, F. Liu, *Nat. Commun.* **2021**, 12, 332.
- [21] J. Wan, Y. Wu, R. Sun, J. Qiao, X. Hao, J. Min, *Energy Environ. Sci.* **2022**, 15, 5192.
- [22] X. Song, K. Zhang, R. Guo, K. Sun, Z. Zhou, S. Huang, L. Huber, M. Reus, J. Zhou, M. Schwartzkopf, S. V. Roth, W. Liu, Y. Liu, W. Zhu, P. Müller-Buschbaum, *Adv. Mater.* **2022**, 34, 2200907.
- [23] Z. Gan, L. Wang, J. Cai, C. Guo, C. Chen, D. Li, Y. Fu, B. Zhou, Y. Sun, C. Liu, J. Zhou, D. Liu, W. Li, T. Wang, *Nat. Commun.* **2023**, 14, 6297.
- [24] J. Wang, Y. Wang, P. Bi, Z. Chen, J. Qiao, J. Li, W. Wang, Z. Zheng, S. Zhang, X. Hao, J. Hou, *Adv. Mater.* **2023**, 35, 2301583.
- [25] J. Song, Y. Li, Y. Cai, R. Zhang, S. Wang, J. Xin, L. Han, D. Wei, W. Ma, F. Gao, Y. Sun, *Matter*. **2022**, 5, 4047.
- [26] K. Hu, C. Zhu, K. Ding, S. Qin, W. Lai, J. Du, J. Zhang, Z. Wei, X. Li, Z. Zhang, L. Meng, H. Ade, Y. Li, *Energy Environ. Sci.* **2022**, 15, 4157.
- [27] J. Qin, Q. Yang, J. Oh, S. Chen, G. O. Oduombaku, N. A. N. Ouedraogo, C. Yang, K. Sun, S. Lu, *Adv. Sci.* **2022**, 9, 2105347.
- [28] W. Zhang, Y. Wu, R. Ma, H. Fan, X. Li, H. Yang, C. Cui, Y. Li, *Angew. Chem., Int. Ed.* **2023**, 62, 202309713.
- [29] L. Kong, Z. Zhang, N. Zhao, Z. Cai, J. Zhang, M. Luo, X. Wang, M. Chen, W. Zhang, L. Zhang, Z. Wei, J. Chen, *Adv. Energy Mater.* **2023**, 13, 2300763.
- [30] S. Bao, H. Yang, H. Fan, J. Zhang, Z. Wei, C. Cui, Y. Li, *Adv. Mater.* **2021**, 33, 2105301.
- [31] L. Chen, J. Yi, R. Ma, L. Ding, T. A. Dela Peña, H. Liu, J. Chen, C. Zhang, C. Zhao, W. Lu, Q. Wei, B. Zhao, H. Hu, J. Wu, Z. Ma, X. Lu, M. Li, G. Zhang, G. Li, H. Yan, *Adv. Mater.* **2023**, 35, 2301231.
- [32] L. Zhong, S.-H. Kang, J. Oh, S. Jung, Y. Cho, G. Park, S. Lee, S.-J. Yoon, H. Park, C. Yang, *Adv. Funct. Mater.* **2022**, 32, 2201080.
- [33] B. Liu, W. Xu, R. Ma, J.-W. Lee, T. A. Dela Peña, W. Yang, B. Li, M. Li, J. Wu, Y. Wang, C. Zhang, J. Yang, J. Wang, S. Ning, Z. Wang, J. Li, H. Wang, G. Li, B. J. Kim, L. Niu, X. Guo, H. Sun, *Adv. Mater.* **2023**, 35, 2308334.
- [34] R. Yu, R. Shi, Z. He, T. Zhang, S. Li, Q. Lv, S. Sha, C. Yang, J. Hou, Z. a. Tan, *Angew. Chem., Int. Ed.* **2023**, 62, 202308367.
- [35] M. Zhou, C. Liao, Y. Duan, X. Xu, L. Yu, R. Li, Q. Peng, *Adv. Mater.* **2023**, 35, 2208279.
- [36] X. Huang, Y. Cheng, Y. Fang, L. Zhang, X. Hu, S. Y. Jeong, H. Zhang, H. Y. Woo, F. Wu, L. Chen, *Energy Environ. Sci.* **2022**, 15, 4776.
- [37] R. Sun, T. Wang, X. Yang, Y. Wu, Y. Wang, Q. Wu, M. Zhang, C. J. Brabec, Y. Li, J. Min, *Nat. Energy*. **2022**, 7, 1087.
- [38] Y. Wei, Z. Chen, G. Lu, N. Yu, C. Li, J. Gao, X. Gu, X. Hao, G. Lu, Z. Tang, J. Zhang, Z. Wei, X. Zhang, H. Huang, *Adv. Mater.* **2022**, 34, 2204718.
- [39] Y. Sun, L. Nian, Y. Kan, Y. Ren, Z. Chen, L. Zhu, M. Zhang, H. Yin, H. Xu, J. Li, *Joule*. **2022**, 6, 2835.
- [40] J. Wang, C. Han, S. Wen, F. Bi, Z. Hu, Y. Li, C. Yang, X. Bao, J. Chu, *Energy Environ. Sci.* **2023**, 16, 2327.
- [41] C. Cao, H. Wang, D. Qiu, T. Zhao, Y. Zhu, X. Lai, M. Pu, Y. Li, H. Li, H. Chen, F. He, *Adv. Funct. Mater.* **2022**, 32, 2201828.
- [42] J. Wan, L. Zeng, X. Liao, Z. Chen, S. Liu, P. Zhu, H. Zhu, Y. Chen, *Adv. Funct. Mater.* **2022**, 32, 2107567.
- [43] S. Liu, H. Li, X. Wu, D. Chen, L. Zhang, X. Meng, L. Tan, X. Hu, Y. Chen, *Adv. Mater.* **2022**, 34, 2201604.
- [44] H. Ning, Q. Jiang, P. Han, M. Lin, G. Zhang, J. Chen, H. Chen, S. Zeng, J. Gao, J. Liu, F. He, Q. Wu, *Energy Environ. Sci.* **2021**, 14, 5919.
- [45] H. Fu, Z. Peng, Q. Fan, F. R. Lin, F. Qi, Y. Ran, Z. Wu, B. Fan, K. Jiang, H. Y. Woo, G. Lu, H. Ade, A. K. Y. Jen, *Adv. Mater.* **2022**, 34, 2202608.
- [46] C. McDowell, M. Abdelsamie, M. F. Toney, G. C. Bazan, *Adv. Mater.* **2018**, 30, 1707114.
- [47] L. Chen, R. Ma, J. Yi, T. A. Dela Peña, H. Li, Q. Wei, C. Yan, J. Wu, M. Li, P. Cheng, H. Yan, G. Zhang, G. Li, *Aggregate*. **2023**, e455.
- [48] J. Lv, H. Tang, J. Huang, C. Yan, K. Liu, Q. Yang, D. Hu, R. Singh, J. Lee, S. Lu, G. Li, Z. Kan, *Energy Environ. Sci.* **2021**, 14, 3044.
- [49] Q. Zhu, J. Xue, G. Lu, B. Lin, H. B. Naveed, Z. Bi, G. Lu, W. Ma, *Nano Energy*. **2022**, 97, 107194.
- [50] G. Ding, T. Chen, M. Wang, X. Xia, C. He, X. Zheng, Y. Li, D. Zhou, X. Lu, L. Zuo, Z. Xu, H. Chen, *Nano-Micro Lett.* **2023**, 15, 92.
- [51] R. Yu, G. Wu, Y. Cui, X. Wei, L. Hong, T. Zhang, C. Zou, S. Hu, J. Hou, Z. a. Tan, *Small*. **2021**, 17, 2103497.
- [52] X. Cui, H. Li, H. Lu, Y. Liu, G. Ran, R. Liu, H. Zhang, X. Ma, D. Li, Y. Lin, J. Yu, W. Zhang, L. Cai, Y. Liu, P. Cheng, A. Zhang, Z. Ma, G. Lu, Z. Bo, *Sci. China Chem.* **2023**, <https://doi.org/10.1007/s11426-023-1821-y>.
- [53] C. He, Y. Pan, G. Lu, B. Wu, X. Xia, C.-Q. Ma, Z. Chen, H. Zhu, X. Lu, W. Ma, L. Zuo, H. Chen, *Adv. Mater.* **2022**, 34, 2203379.
- [54] X. Xu, L. Yu, H. Meng, L. Dai, H. Yan, R. Li, Q. Peng, *Adv. Funct. Mater.* **2022**, 32, 2108797.
- [55] L. Wang, C. Chen, Y. Fu, C. Guo, D. Li, J. Cheng, W. Sun, Z. Gan, Y. Sun, B. Zhou, C. Liu, D. Liu, W. Li, T. Wang, *Nat. Energy*. **2024**, 9, 208.
- [56] Y. Wang, J. Xue, H. Zhong, C. R. Everett, X. Jiang, M. A. Reus, A. Chumakov, S. V. Roth, M. A. Adediji, N. Jili, K. Zhou, G. Lu, Z. Tang, G. T. Mola, P. Müller-Buschbaum, W. Ma, *Adv. Energy Mater.* **2023**, 13, 2203496.

- [57] R. Ma, C. Yan, P. W.-K. Fong, J. Yu, H. Liu, J. Yin, J. Huang, X. Lu, H. Yan, G. Li, *Energy Environ. Sci.* **2022**, *15*, 2479.
- [58] C. Guo, D. Li, L. Wang, B. Du, Z.-X. Liu, Z. Shen, P. Wang, X. Zhang, J. Cai, S. Cheng, C. Yu, H. Wang, D. Liu, C.-Z. Li, T. Wang, *Adv. Energy Mater.* **2021**, *11*, 2102000.
- [59] C. Guo, Y. Fu, D. Li, L. Wang, B. Zhou, C. Chen, J. Zhou, Y. Sun, Z. Gan, D. Liu, W. Li, T. Wang, *Adv. Mater.* **2023**, *35*, 2304921.
- [60] X. Jiang, A. J. Gillett, T. Zheng, X. Song, J. E. Heger, K. Sun, L. V. Spanier, R. Guo, S. Liang, S. Bernstorff, P. Müller-Buschbaum, *Energy Environ. Sci.* **2023**, *16*, 5970.
- [61] T. A. Dela Peña, R. Ma, Y. Luo, Z. Xing, Q. Wei, Y. Hai, Y. Li, S. A. Garcia, K. L. Yeung, T. Jia, K. S. Wong, H. Yan, G. Li, M. Li, J. Wu, *Adv. Energy Mater.* **2024**, *14*, 2303169.
- [62] Y. Liu, J. Zhang, C. Tian, Y. Shen, T. Wang, H. Zhang, C. He, D. Qiu, Y. Shi, Z. Wei, *Adv. Funct. Mater.* **2023**, *33*, 2300778.
- [63] B. Fan, W. Zhong, W. Gao, H. Fu, F. R. Lin, R. W. Y. Wong, M. Liu, C. Zhu, C. Wang, H.-L. Yip, F. Liu, A. K. Y. Jen, *Adv. Mater.* **2023**, *35*, 2302861.
- [64] Z. Liang, L. Yan, N. Wang, J. Si, S. Liu, Y. Wang, J. Tong, J. Li, B. Zhao, C. Gao, X. Hou, *Adv. Funct. Mater.* **2023**, 2310312.
- [65] D. Jiang, J. Sun, R. Ma, V. K. Wong, J. Yuan, K. Gao, F. Chen, S. K. So, X. Hao, G. Li, H. Yin, *Mater. Sci. Eng.: R: Rep.* **2024**, *157*, 100772.
- [66] R. Ma, Q. Fan, T. A. Dela Peña, B. Wu, H. Liu, Q. Wu, Q. Wei, J. Wu, X. Lu, M. Li, W. Ma, G. Li, *Adv. Mater.* **2023**, *35*, 2212275.
- [67] Y. Tamai, Y. Murata, S.-i. Natsuda, Y. Sakamoto, *Adv. Energy Mater.* **2024**, *14*, 2301890.
- [68] T. A. Dela Peña, R. Ma, Z. Xing, Q. Wei, J. I. Khan, R. M. Young, Y. Hai, S. A. Garcia, X. Zou, Z. Jin, F. L. Ng, K. L. Yeung, D. F. Swearer, M. R. Wasielewski, J. Wang, H. Cha, H. Yan, K. S. Wong, G. Li, M. Li, J. Wu, *Energy Environ. Sci.* **2023**, *16*, 3416.
- [69] R. Ma, H. Li, T. A. Dela Peña, X. Xie, P. W.-K. Fong, Q. Wei, C. Yan, J. Wu, P. Cheng, M. Li, G. Li, *Adv. Mater.* **2024**, *36*, 2304632.
- [70] L. Zhang, Q. Du, D. Zhou, P. Zhou, *Sci. Total Environ.* **2022**, *808*, 151868.
- [71] J. Guo, S. Ali, M. Xu, *Green Carbon.* **2023**, *1*, 150.